Facile fabrication of Ni-Fe-layered double hydroxide for boosted adsorption of Alizarin Red S dye in water

Mohamed Ismail*,1, Hédi Ben Amor1 and Ridha Djellabi*,2

1Processes, Energetic, Environment and Electric Systems (PEESE), National School of Engineers, Gabes University, Gabes 6072, Tunisia

2Department of Chemical Engineering, Universitat Rovira i Virgili, 43007, Tarragona, Spain

Corresponding authors: M. Ismail: ismail.issatg@gmail.com; R. Djellabi: ridha.djellabi@urv.cat

Abstract

This work aims to design layered double hydroxide (Ni-Fe-CO$_3$) via simple co-precipitation route for the elimination of Alizarin Red S (ARS) dye from water. The physicochemical properties of Ni-Fe-CO$_3$ adsorbent were studied using different spectroscopic and analytical techniques. The adsorptive ability of Ni-Fe-CO$_3$ was evaluated for the removal of ARS under different conditions in order to understand the mechanistic pathways. Ni-Fe-CO$_3$ showed high adsorption capacity up to 454.45 mg/g within just 1 h. It was found that the raise in the medium temperature from 20°C to 40°C boosts the adsorption ability, while above this value, there was no change in the adsorption capacity. The capacity of adsorption was found to be 157.97 to 55.38 mg/g at pH 2 to 9, respectively. The surface chemistry of the adsorbent and the dye charge in solution are significantly responsible for the pH dependency of dye adsorption. The analysis of adsorption data utilized different isotherm models shows that Freundlich isotherm is the most pertinent to the adsorption process. In accordance with the kinetic studies, the pseudo-second-order kinetic model, which also takes into account intra-particle diffusion in the adsorption process, may adequately describe the behavior of adsorption. The thermodynamic characteristics, such as ΔH°, ΔS°, and ΔG°, were found to be endothermic, spontaneous, and practicable. Even through the synthesis process is simple via the use of low-cost elements, the adsorption ability was comparatively high compared to the previous reported materials. Bridging between the lost cost of the process and high effectiveness is the best way to transfer the use of emerging materials to real world use.

Keywords: Ni-Fe-layered double hydroxide; Alizarin Red S; Adsorption isotherms; Water treatment; Dye removal.

INTRODUCTION

The huge discharge of organic dyes in the environment has led to several health and environmental issues. Dyes are mostly discharged by leather, printing, plastics and textiles industries [1-3]. The toxic effect of dyes directly affects the photosynthetic activity in aquatic life [4, 5]. As a consequence, the risk of these dyes is transferred to the whole ecosystem and human health [6, 7]. The necessity to cleanse these effluents before disposal is therefore required. Several wastewater treatment technologies can be used to treat textile wastewater in a variety of ways, such as adsorption [8], nanofiltration membrane [9], photocatalysis [10-12], sonolysis [13], and electrochemical approaches [14]. Adsorption is a simple and a safe technique to remove different pollutants including organic pollutants [15], heavy metals [16, 17] and inorganic compounds [18] from wastewaters.

Activated carbon is the typical employed material for many decades to purify wastewater by adsorption. However, over the recent years, the cost of activated carbon is raising, as well as its regeneration maybe costly and difficult. Numerous research studies have been achieved to examine the use of cheap materials derived from various agricultural by-products [19], such as date stones [20], wood shaving [21], palm petiole [22] and so on.

Over recent years, the design of layered double hydroxides (LDHs) has significantly attracted the scientific community because of their physical and structural proprieties such as high surface area and interlayer ion exchange [23, 24]. LDHs recognized as anionic clays represent an essential group of ionic lamellar solids [25], with the formula $[M^{2+}_{1-x}M^{3+}_x(OH)_2]_x^+(A^{n-})_{x/n}$. mH_2O, wherein M^{2+} and M^{3+} are metallic species and A^{n-} is an exchangeable anion [26]. LDHs showed excellent adsorptive ability toward the removal of dyes and pigments from aqueous solutions [27, 28]. Rodrigo et al. [29] prepared Ma/Al layered double hydroxide (LDH) composites and they compared the calcined and uncalcined samples for Acid Green 68:1 adsorption. It was found that the adsorption capacity reaches 99.1, and 154.8 mg g^{-1}, respectively. The elements used to construct LDH based materials are crucial as they affect directly the morphological, structural and functionality characteristics, which in turn affect the adsorption ability. The purpose of this study is to design Ni and Fe LDH based adsorbent having high stability and adsorptive capacity. It is believed that the route of synthesis matters significantly for developing economic and effective based materials. Three main factors must be taken into consideration to develop a product that can be used at large scale including the cost of starting materials and synthesis reagents, the performance of the obtained adsorbent and its stability, and the sustainability of the overall process [30]. Herein, Fe and Ni were used to design LDH adsorbent for the removal of anionic dye (Alizarin Red S (ARS) ARS is generally used in textile industries. It is less biodegradable and highly toxic effect towards the environment [31]. The removal of ARS from water has been studied by several routes including Fenton oxidation [32], ultrasound enhanced electrochemical oxidation [33], catalytic ozonation [34], anodic oxidation [35], photocatalysis [36], adsorption [37] and so on. These techniques have their own cons and pros in terms of efficiency, cost and sustainability. In our study, we focused on the removal of ARS by low-cost designed Ni-Fe-LDH. The effects of some factors including pH, contact time, mass of adsorbent and temperature on the removal of ARS were studied in detail. Adsorption isotherms, kinetic models and adsorption mechanisms were developed from experimental data.

Experimental

Materials and reagents

$FeCl_3.6H_2O$, Na_2CO_3, $NiCl_2.6H_2O$ and NaOH (Sigma-Aldrich) were used. Alizarin Red S (abbreviated as ARS) is considered as an anionic dye. The dye's physicochemical characteristics are listed in Table 1.

Table 1. Physiochemical properties of the dye Alizarin red S

Parameter	values
Molecular weight	342.26 g mol^{-1}
Molecular formula	$C_{14}H_7NaO_7S$
Solubility in water	1mg mL^{-1} (20 °C)
Color Index Number	58005
Absorption maxima	420 nm (at pH below3.7)
pKa	4.5
Synonym	3,4-Dihydroxy-9,10-dioxo-2-anthracenesulfonicacidsodium salt.

LDH synthesis

According to Reichle's approach, Ni-Fe-LDH was designed using the co-precipitation route at pH 11 [38]. A mixed aqueous solution of NiCl$_2$.6H$_2$O (0.2 mol) and FeCl$_3$.6H$_2$O (0.1 mol), with Ni^{2+}/Fe^{3+} molar ratio of 2 in distilled water (100 mL) was introduced dropwise under active stirring into 100 mL solution (0.2 mol of Na$_2$CO$_3$ and 0.1 mol of NaOH) at room temperature. By adding 3M NaOH solution, the pH kept constant during the co-precipitation process at a value of 11. After that, the mixture was kept under continuous stirring for 24 h at 80°C for maturation, and then the suspension was recovered by centrifugation. Ni-Fe-LDH was washed and dried at 80 °C for a day. The material was characterized by FFTIR, XRD,

Adsorption experiments

In 250 mL beakers with a predefined mass of adsorbent and 100 mL dye-solution with various concentrations, a batch adsorption study of the dye ARS onto LDHs was conducted; the working solution was stirred at the room temperature. The concentration of ARS was followed by spectrophotometrically at 430 nm. The capacity of adsorption and removal rates were by equations reported elsewhere [39].
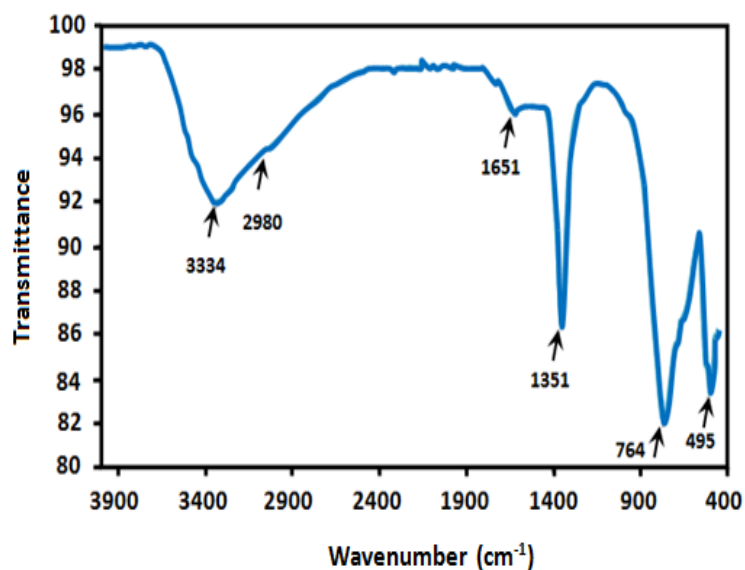
Characterisation analysis

The functional groups of Ni-Fe-LDH were identified using FTIR, Bruker-Vertex 70, KBr pellet technique. The crystallinity of the Ni-Fe-LDH as determined using an X-ray diffractometer (XRD, PANalytical Empyrean, Netherlands) with Cu-K radiation (1.5406 Å. The pH of the zero-point charge (pHpzc) was opted by the method proposed by Yang [40] by setting pH at different values from 2 to 12, while, the pHpzc of the sample was determined at the pH$_{final}$ = pH$_{initial}$ value.

RESULTS AND DISCUSSION

**Characterization of Ni-Fe-LDH**

Spectroscopy analysis

Figure 1 depicts the infrared spectrum of the Ni-Fe-LHD between 4000 and 400 cm^{-1}. Hydrotalcite-type elements with CO$_3^{2-}$ as the counter anions were observed [41]. The broad band at 3344 cm^{-1} is associated to hydroxyl groups and H$_2$O, while the weak bond at 1651 cm^{-1} is due to O-H stretching [42]. The characteristic vibrational mode of the CO$_3^{2-}$ can be observed at 1351 cm^{-1}. Low frequency bands (below 1000 cm^{-1}) in brucite-type layers are associated to Fe-O, Ni-O, and vibrational modes metal oxides [43, 44].

Figure 1. FTIR spectrum of prepared Ni-Fe LDH.

XRD pattern analysis

Figure 2 shows powder X-ray diffraction spectrum of Ni-Fe LDH. The solid's XRD characterization revealed the produced peaks are due to the formation of well-crystallized phase LDH. Major peaks of the Ni-Fe-LDH were positioned at approximately 11.6°, 23.4°, 34.5°, 39.1°, 47.5°, 60°, 61.3° and 65.5°. These peaks can be attributed respectively to planes (003), (006), (012), (015), (018), (110), (113) and (116 [41]. XRD spectrum confirms the successful synthesis of Ni-Fe LDH by the used route.
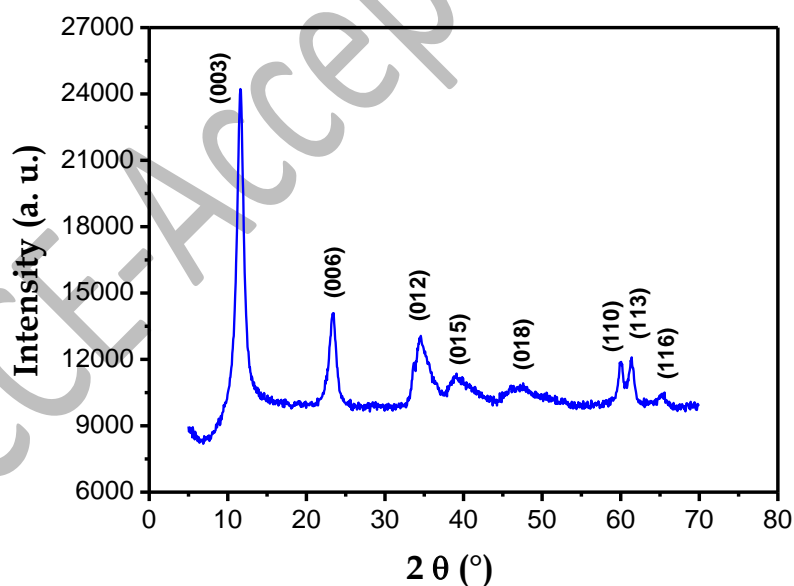

Figure 2. X-ray diffraction of Ni-Fe LDH

pHpzc of Ni-Fe-LDH

pHpzc for Ni-Fe-LDH was around 7.7 (Figure 3). pHpzc provides important information about the charge of the adsorbent at different pH values. At pH below the PZC, the LDH surface is positively charged (pH < pHpzc), and at pH is above the PZC, it is negatively charged (pH > pHpzc). It is important to point out that the attraction and

adsorption different pollutant species depends significantly on the charge of adsorbent against the charge of pollutants, wherein electrostatic effects take place [45].
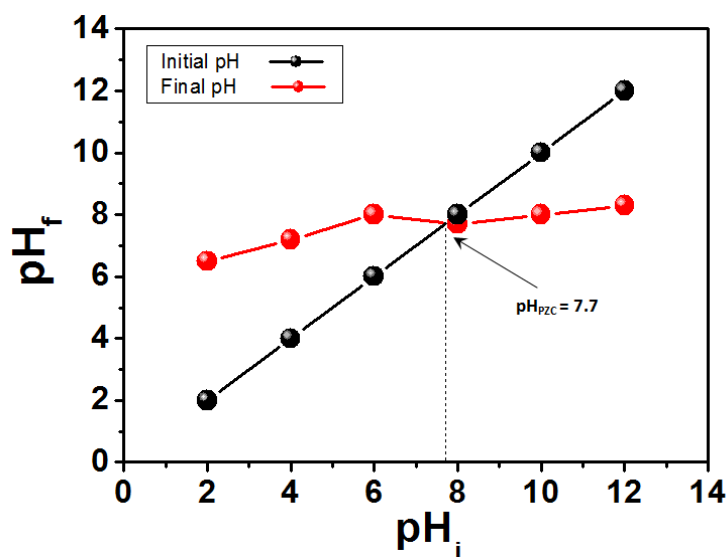

Figure 3. Point of zero charge (pHpzc) for Ni-Fe LDH

## Adsorption study

Effect of pH

pH has a direct effect on the sorption of pollutants on the surface of adsorbents based on the electrostatic attractions [46]. Herein the influence of pH was studied at pH values from 2 to 9 at 100 mg/L of initial concentration, 0.25 g/L of Ni-Fe LDH, at 25 °C. As indicated in Figure 4, the equilibrium adsorption (Qe) decreases with rising pH solution, from 157.97 to 55.38 mg/g when the pH increases from 2 to 9. The characteristics of Ni-Fe LDH adsorbent and chemistry of ARS in solution are significantly responsible as function of pH values. If the pH is lower, more H^+ ions build up on the adsorbent surface, which increases the electrostatic contact between the anionic sulfonate groups of ARS (ARS-SO_3^-) and the positively charged adsorbent surface. Higher pH values (pH > pHpzc) may result in a reduction in the adsorption of ARS due to a reduction in electrostatic attraction. Because the adsorbent's surface was negatively charged, negatively charged dye ions tended to be repelled by it via electrostatic repulsion, which reduced the adsorption capacity. Meanwhile, the competition between the dye species and OH⁻ ions in aqueous solution for the adsorption sites was also causes the reduction of dye removal. Adjusting of solution pH can enhance the adsorption selectivity as reported by many studies. In addition, the development of multi-layer adsorption is associated directly to solution pH [47, 48].
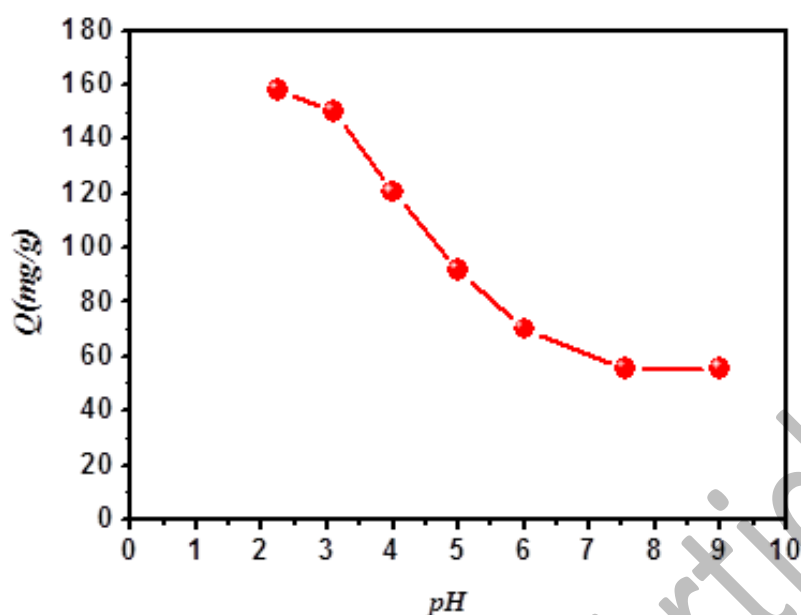
Figure 4. pH effect on ARS adsorption on the surface Ni-Fe LDH, [ARS]: 100 mg L^{-1}, V=100 mL, Ni-Fe LDH dose 25 mg and contact time 1h at room temperature.

Effect of ARS concentration

Figure 5 displays the ARS adsorbed quantity on the surface of Ni-Fe-LDH at various initial ARS doses within the range 40-100 mg L^{-1}. According to the kinetic study, dye elimination gets faster with time and reaches saturation in around 60 minutes. The amount of ARS adsorbed increased rapidly in the initial stage and then progressively became slower until the equilibrium was reached. Many free adsorptive sites on the surface of LDH that is ready for adsorption during the first phase, which boosts the fast fixation of dye molecules. When the surface gets saturated with dye molecules, less interaction and fixation of ARS by ion exchange process was found at contact time around 1 h [49].
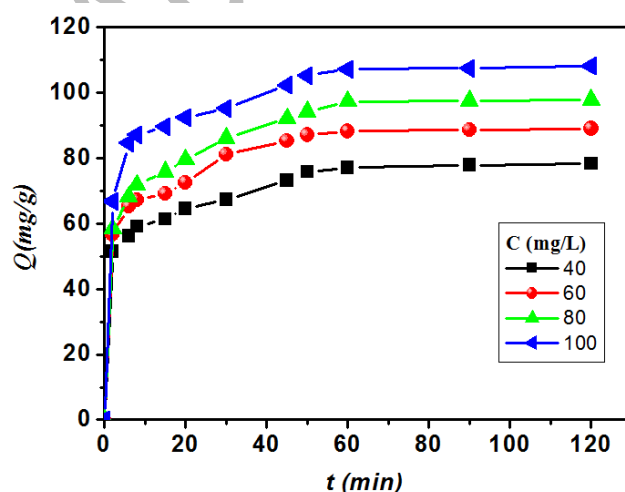
Figure 5. Effect of contact time on the adsorption of ARS on Ni-Fe LDH, [ARS]: 100 mg L^{-1}, pH 2, and Ni-Fe LDH mass 80 mg, V=100 mL.

Effect of Ni-Fe LDH dose

The HDL dose effect on the adsorption was carried out by changing the quantity of adsorbent ranging from 25 to 150 mg. Figure 6 demonstrates that the dye adsorption increases quickly with increasing adsorbent mass, reaching a maximum at 80 mg for ARS dye. This may be because there were more empty sites available. After reaching this maximum equilibrium value, increasing adsorbent mass had no further effect on the removal ability [50, 51]. With an increase in HDL dosage from 25 to 80 mg, the adsorption rate increases from 39.5 to 92.7%. However, above 80 mg, the adsorption rate remains stable at around 93%. At lower masses (25 to 80 mg), the adsorption of dye is proportional to the adsorbent mass, as the mass increases more available adsorptive sites are obtained to fix the pollutant. From masses ranging from 80 to 15 mg, the adsorption rates are similar even though more adsorptive sites are expected to be available. However, the aggregation of particles at higher mass values could take place which reduces the surface area of adsorbent particles. On top of that, when the concentration of dye molecules is relatively low, the fixation of ARS on Ni-Fe LDH surface becomes difficult due to the less mass transfer.
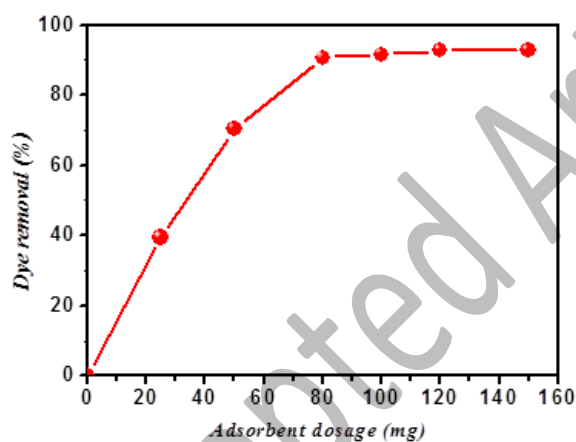
Figure 6. Adsorption rate as a function of adsorbent mass, pH: 2, 100 mg L^{-1}, V=100 mL.

Effect of temperature

The influence of temperature on ARS removal was carried out at different temperature values and the obtained results shown in Figure 7. The amount of Alizarin red S dye adsorbed increased when temperature increases from 20°C to 40°C, and then there was no observed effect on the adsorption with the raise of temperature from to 40 to 60°C. Within the range 20°C to 40°C, the adsorption rate increases due to the enhanced mass transfer. Dye molecules could access faster to the adsorptive sites when the solution is heated through the decrease in the viscosity degree of the solution [52]. On top of that, by increasing the temperature of the medium, the boundary layer around the adsorbent particles, which limits the access of pollutant molecules, can be reduced or destroyed, boosting the interaction between the Ni-Fe LDH and the pollutant species [53]. At temperature ranging from 40 to 60°C, there was not observed effect on the adsorption process which could be explained probably by reaching the maximum mass transfer catalysed by the temperature.
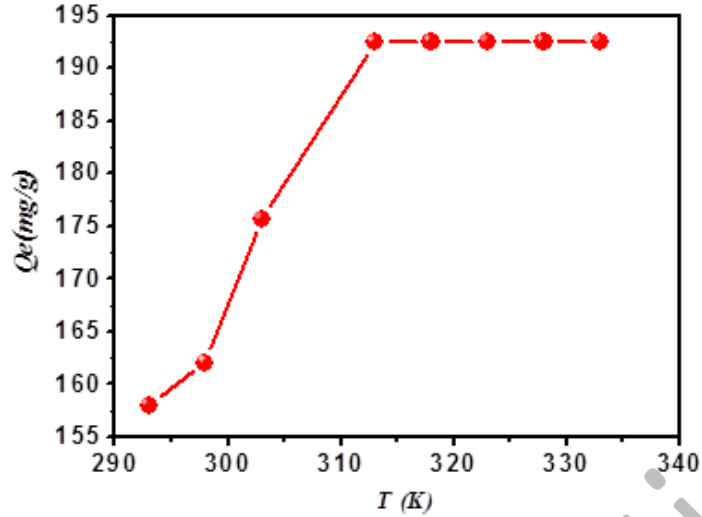
Figure 7. Effects of temperature on the removal of ARS on Ni-Fe LDH at initial dye concentration 100 mg L^{-1}; m$_{HDL}$=25mg, V=100 mL; pH=2; T=25°C ; t=1h).

Adsorption isotherms

To understand the mechanism of ARS adsorption on Ni-Fe-LDH, Langmuir [54], Freundlich [55] and Temkin [56] isotherm models were used.

In terms of Langmuir adsorption model, once a pollutant resides at a location, no additional adsorption can occur there. The linear form of Langmuir isotherm (Eq. (3)) can be expressed as:

$$\frac{C_e}{q_e} = \frac{1}{K_L q_{max}} + \frac{C_e}{q_{max}} \tag{3}$$

Where q$_e$ and C$_e$ are the amount of ARS fixed on the surface of adsorbent (g) and equilibrium concentration of ARS remained in solution, respectively. In Eq. (3), q$_{max}$ presents the predicted monolayer adsorption capacity (mg g^{-1}) and K$_L$ is the equilibrium constant (Lmg^{-1}).

The Freundlich model presupposes that multilayer adsorption is how dye molecules are absorbed onto heterogeneous surfaces. The linearized equation describing the Freundlich isotherm is shown by Eq. (4):

$$ln q_e = \frac{1}{n} ln C_e + ln K_F \tag{4}$$

K$_F$ is the capacity of adsorption and 1/n is the adsorption intensity.

The adsorption heterogeneous system is described by the Temkin isotherm. It is based on the hypothesis that adsorption heat linearly reduces as adsorption capacity increases. It is expressed by Eq. (5) below

$$q_e = Bln A + Bln C_e \tag{5}$$

Where B = RT/b, a constant associated to the heat of adsorption. R is the gas constant (8.314 J/mol K), T is the absolute temperature (K), b is the Temkin constant (J/mol) and A is the Temkin isotherm constant (L/g). By evaluating the correlation coefficients, the appropriate isotherm models to match the adsorption data were contrasted, R^2. The closer the R^2 value to unit, the better the fit. At room temperature and pH 2, the adsorption isotherms for ARS were investigated using initial ARS concentrations of 100 to 600 mg. L^{-1}. Figure 8 presents graphical representations of the isotherm models. The parameters of Langmuir, Freundlich, and Temkin can be obtained from the slope and intercept of each linear plot and are shown in Table 2 with appropriate correlations. The results indicated that the R^2 value in the case of Freundlich isotherm is superior to those in cases of Langmuir

and Temkin. Thus, it may be said that multilayer adsorption techniques allow for the determination of ARS adsorption onto Ni-Fe- HDL. Multilayer adsorption is very beneficial for the adsorption of pollutants by adsorption from water, which usually leads to high adsorption capacity. In fact, multilayer adsorption usually reflects a high adsorption capacity as compared to monolayer based adsorption.

Table 2. Constants and coefficients of different isotherm models for adsorption of ARS onto Ni-Fe-LDH

	Langmuir			Freundlich			Temkin		
	q_m (mg g^{-1})	K_L	R^2	K_F(mg/g)(mg/L)^n	n	R^2	B_T	K_T	R^2
Ni-Fe-LDH	454.545	0.020	0.948	52.677	2.837	0.987	78.69	0.393	0.919
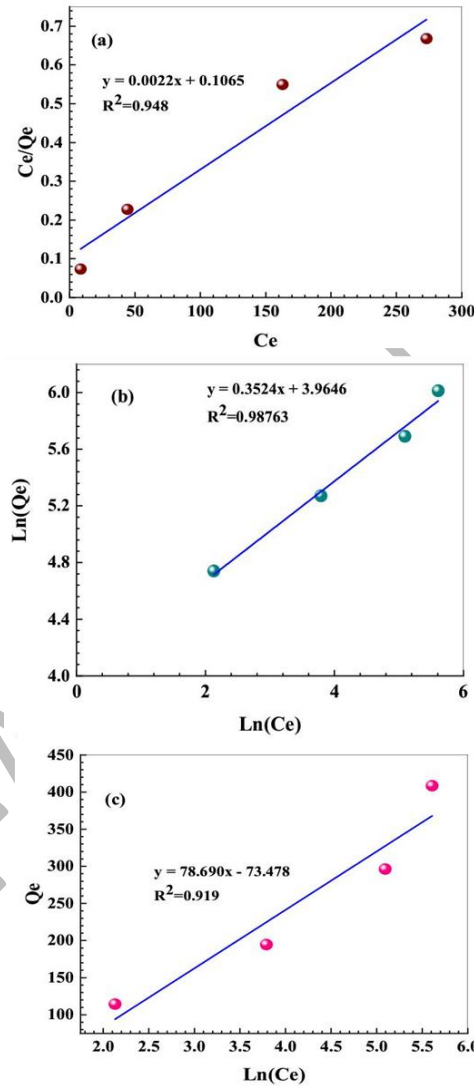
Figure 8. Curves of (a) Langmuir (b) Freundlich (c) Temkin isotherm models

Adsorption kinetics studies

Two models, Lagergren pseudo-first-order model (Eq. (6)) and the pseudo-second-order model (Eq. (7)), [57] were applied to investigate the kinetics of the adsorption of ARS dye onto Ni-Fe-LDH.

$$\ln(q_e - q_t) = \ln q_e - k_1 t \tag{6}$$

$$\frac{t}{q_t} = \frac{1}{k_2 q_e^2} + \frac{t}{q_e} \tag{7}$$

Where (q_e) and (q_t) (mg g^{-1}) are the capacities of adsorption at equilibrium and at time t, respectively, k_1 is the equilibrium rate constant of pseudo-first-order adsorption (min^{-1}) and k_2 (g mg^{-1}min^{-1}) is the pseudo-second-order rate constant.

Figure 9 shows the representation of the pseudo-first-order and pseudo-second-order linearized forms. Equilibrium adsorption qe and kinetic model parameters were calculated using the slopes and intercepts of plots. The values of the correlation coefficient (R^2) and parameters are shown in Table 3. The pseudo-second-order model shows superior R^2 values than those obtained by pseudo-first-order model. Furthermore, the second order kinetic model predicts an equilibrium adsorption $q_{e,th}$ that is closer to the experimentally reported equilibrium adsorption, demonstrating that the pseudo-second-order kinetic model better represents the ARS adsorption kinetics of Ni-Fe-LDH.

To understand the mechanisms and rate-limiting phases which affect the adsorption kinetics, it was found the experimental data of adsorption kinetics can be fitted to the Weber's intra-particle diffusion model [58], which is expressed as:

$$q_t = k_p t^{1/2} + C \tag{8}$$

Where C (mg g^{-1}) is a parameter relating to the boundary layer thickness and kp (mg g^{-1} min$^{-1/2}$) denotes the intra-particle diffusion rate constant. According to this kinetic model, intra-particle diffusion is the only rate-limiting phase if the plot of qt versus t$^{1/2}$ is linear and crosses the origin. On the other hand, if this plot does not pass through the origin and showed multilinearity, then two or more steps, such as exterior diffusion, pore diffusion, and adsorption on the internal surface of the adsorbent, were involved.

Figure 10 displays a visualization of the intra-particle diffusion model's linearized version.

Table 3. Adsorption kinetic parameters of ARS on Ni-Fe-LDH

C_0	qe,exp	Pseudo-first-order			Pseudo-second-order		
mg L^{-1}	mg g^{-1}	$K_1(min^{-1})$	$q_{e,th}(mgg^{-1})$	R^2	$K_2(min^{-1}mg^{-1}min^{-1})$	$q_{e,th}(mgg^{-1})$	R^2
40	77.9	0.052	39.40	0.955	0.0043	80.00	0.998
60	88.7	0.057	43.93	0.953	0.0042	90.90	0.998
80	97.5	0.062	57.85	0.939	0.0033	100.00	0.998
100	107.5	0.051	46.17	0.917	0.0039	109.89	0.998
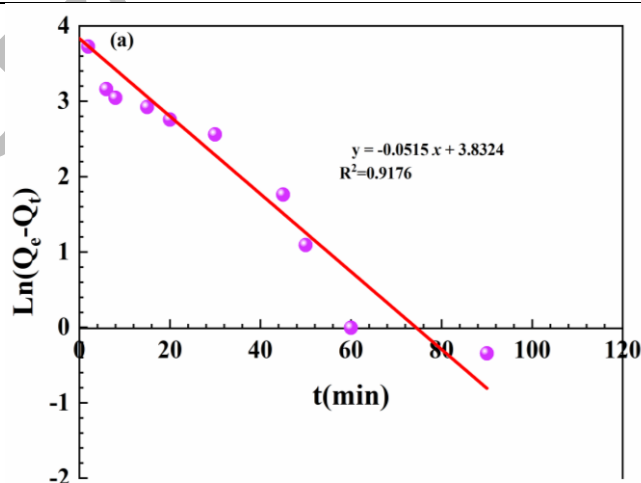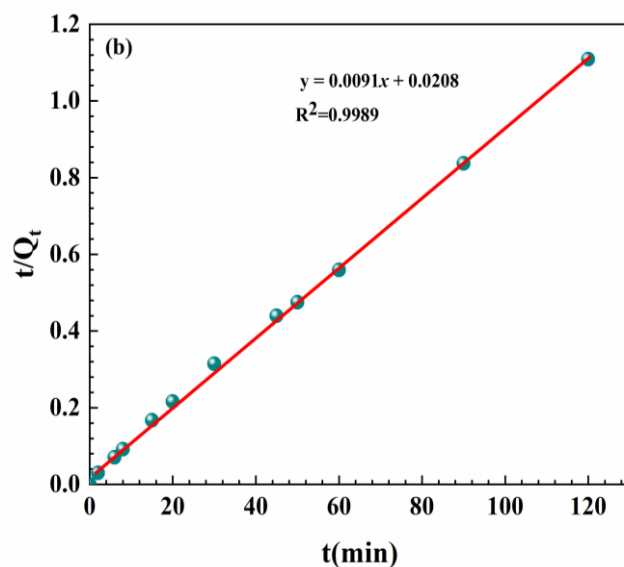
Figure 9. Adsorption kinetics of ARS on Ni-Fe LDH (a) pseudo-first order (b) pseudo-second order, ([ARS]: 100 mg L^{-1}; m$_{HDL}$=80 mg, V=100 mL; pH=2; T=25°C).
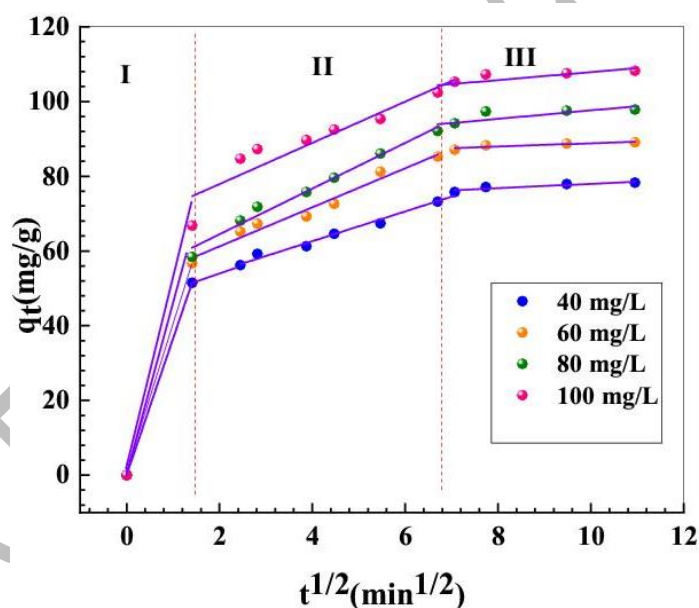
Figure 10. Intraparticle diffusion plots for ARS adsorption on Ni-Fe-LDH.

The plot of qt versus t$^{1/2}$ can be divided into three straight portions for all concentrations, as shown in Figure 10. These portions are due to the rapid external surface adsorption (region I, kpI), gradual intraparticle diffusion (region II, kpII), and the stage of adsorption equilibrium (region III, kpIII). For various starting concentrations, the first step was reached rapidly. The values of the intraparticle diffusion parameters for various phases are listed in Table 4. It is shown that when initial ARS concentrations rise, so do the values of kpI and kpII. Additionally, the fact that the kpI values are higher than the kpII values suggests that the film diffusion is a quick and essential step in the adsorption of ARS onto the NiFe-CO$_3$-LDH.

The last step is a process of thermodynamic equilibrium between adsorption and desorption of ARS [59].

Table 4. Calculated parameters for intra-particle diffusion for adsorption of ARS

C_0 mg L^{-1}	Region I		Region II		Region III	
	Kp_I (mg g^{-1}min$^{-1/2}$)	R^2	Kp_{II} (mg g^{-1}min$^{-1/2}$)	R^2	Kp_{III},(mg g^{-1}min$^{-1/2}$)	R^2
40	40.21	0.998	3.978	0.988	0.440	0.926
60	36.52	0.998	5.220	0.978	0.580	0.802
80	41.40	0.998	5.880	0.986	0.723	0.568
100	47.38	0.998	6.110	0.897	1.013	0.611

Adsorption thermodynamics

The following equations (Eq. (9) and Eq. (10)) were used to calculate the thermodynamic characteristics of the sorption process, including the change in standard free energy ($\Delta G°$), enthalpy ($\Delta H°$), and entropy ($\Delta S°$), from experiments conducted at various temperatures [60].

$$\Delta G° = -RTlnK_D \qquad (9)$$

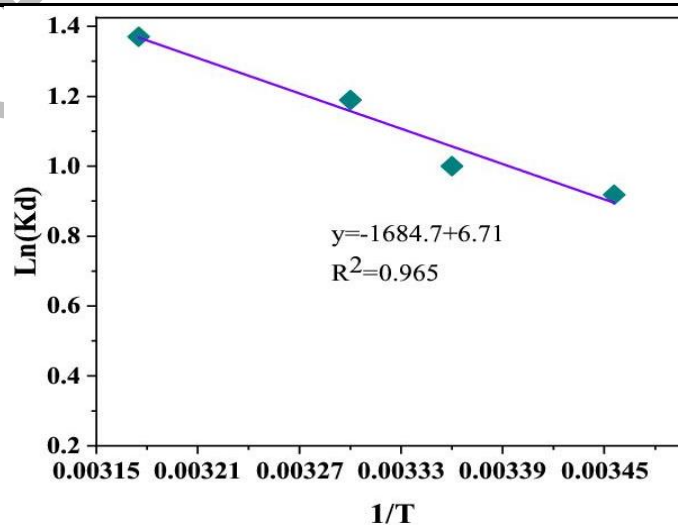$$lnK_D = \frac{\Delta S°}{R} - \frac{\Delta H°}{RT} \qquad (10)$$

Where R is the molar gas constant, T is the temperature (K) and K_D is the coefficient of distribution (quantity of eliminated dye per gram of adsorbent by its concentration in the liquid phase), which is calculated with the following equation:

$$K_D = \frac{q_e}{c_e} \qquad (11)$$

In order to determine the values of $\Delta S°$ and $\Delta H°$, Van't Hoff plots of ln KD versus 1/T's slope and intercept were utilized (Figure 11). The values for ($\Delta G°$), ($\Delta H°$), and ($\Delta S°$) are shown in Table 5. The positive values of $\Delta H°$ and $\Delta S°$ serve as evidence of the endothermic character of the adsorption process with increasing system randomness. Negative free energy values ($\Delta G°$) indicate a spontaneous process.

Table 5. Parameters of thermodynamic values for ARS dye removal with Ni-Fe-LDH.

C_0(mg.L^{-1})	T(K)	$\Delta G°$(KJ.mol^{-1})	$\Delta H°$(KJ.mol^{-1})	$\Delta S°$(J.K^{-1}.mol^{-1})
100	293	-2.289	14.034	55.703
	298	-2.568		
	303	-2.847		
	313	-3.404		

Figure 11. Van't Hoff's fpr of ARS adsorption on the surface of Ni-Fe-LDH

Comparison of ARS adsorption capacities with various adsorbents

Table 6 shows the Ni-Fe-LDH and other adsorbents' capacities for adsorption of ARS. The theoretical maximum adsorption capacity of Ni-Fe-LDH for the adsorption of ARS was 454.45 mg/g, which is far better than most of the adsorbents. According to this comparison study, Ni-Fe-LDH is a promising adsorbent with a lot of promise for removing contaminants from water.

Table 6. Comparison of Ni-Fe-LDH adsorption performance with other materials

Adsorbents	*Adsorption capacity* $(mg\ g^{-1})$	Best fit isotherm	*Reference*
Activated carbon/-Fe_2O_3 nano-composite	108.69	Langmuir	[61]
Mustard husk	1.97	Freundlich	[62]
Olive stone	16.01	Freundlich	[63]
Magnetic chitosan	40.12	Langmuir	[64]
Hexadecyl trimethyl ammonium bromide modified montmorillonite	666.6	Langmuir	[65]
Mg-Al LDH	49.53	Langmuir	[66]
CuAl-LDH	33.44	Langmuir	[67]
Ni-Fe LDH	454.45	Freundlich	This work

CONCLUSIONS

Herein, we studied the adsorption of ARS using low-cost Ni-Fe LDH prepared by simple precipitation. The results show that ARS can be adsorbed quickly on the Ni-Fe-LDH, wherein the equilibrium occurs within 60 minutes. The study showed that Ni-Fe-LDHs can adsorb up to 454 mg/g. The performance of Ni-Fe LDH was studied under different conditions and both the isotherm models and adsorption kinetics were studied. The quick adsorption of ARS dye on Ni-Fe LDH is due to the multilayer adsorption mechanism and the strong electrostatic attraction. The capacity of adsorption was relatively high against most reported adsorbents. The easy synthesis and low-cost of Ni-Fe LDH would make it potential material for the treatment dye-containing wastewaters.

Data availability statement

The data that support the findings of this study are available on request from the corresponding author.

Disclosure statement

No potential conflict of interest was reported by the author(s).

REFERENCES

[1] L. El Gaini, M. Lakraimi, E. Sebbar, A. Meghea, M. Bakasse, Removal of indigo carmine dye from water to Mg–Al–CO3-calcined layered double hydroxides, Journal of Hazardous Materials, 161 (2009) 627-632.

[2] A. Karimi, H. Mohammadi, E. Fatehifar, Evaluation of Textile Wastewater Treatment Using Combined Methods: Factor Optimization via Split Plot RSM, Iranian Journal of Chemistry and Chemical Engineering, 41 (2022) 607-617.

[3] S. Nouacer, R. Djellabi, Easy-handling semi-floating TiO2-based aerogel for solar photocatalytic water depollution, Environmental Science and Pollution Research, 30 (2023) 22388-22395.

[4] M. Liu, Q. Chen, K. Lu, W. Huang, Z. Lü, C. Zhou, S. Yu, C. Gao, High efficient removal of dyes from aqueous solution through nanofiltration using diethanolamine-modified polyamide thin-film composite membrane, Separation and Purification Technology, 173 (2017) 135-143.

[5] R. Djellabi, C.L. Bianchi, M.R. Haider, J. Ali, E. Falletta, M.F. Ordonez, A. Bruni, M. Sartirana, R. Geioushy, Photoactive polymer for wastewater treatment, Nanomaterials for Water Treatment and Remediation; CRC Press: Boca Raton, FL, USA, (2021) 217-244.

[6] J.A. González, M.E. Villanueva, L.L. Piehl, G.J. Copello, Development of a chitin/graphene oxide hybrid composite for the removal of pollutant dyes: adsorption and desorption study, Chemical engineering journal, 280 (2015) 41-48.

[7] S. Abbasi, F. Ahmadpoor, M. Imani, M.-S. Ekrami-Kakhki, Synthesis of magnetic Fe3O4@ ZnO@ graphene oxide nanocomposite for photodegradation of organic dye pollutant, International journal of environmental analytical chemistry, 100 (2020) 225-240.

[8] A. Ahmad, B. Hameed, Reduction of COD and color of dyeing effluent from a cotton textile mill by adsorption onto bamboo-based activated carbon, Journal of hazardous materials, 172 (2009) 1538-1543.

[9] E. Ellouze, N. Tahri, R.B. Amar, Enhancement of textile wastewater treatment process using nanofiltration, Desalination, 286 (2012) 16-23.

[10] S. Abbasi, M.-S. Ekrami-Kakhki, M. Tahari, Modeling and predicting the photodecomposition of methylene blue via ZnO–SnO 2 hybrids using design of experiments (DOE), Journal of materials science: materials in electronics, 28 (2017) 15306-15312.

[11] A.H. Navidpour, M. Fakhrzad, M. Tahari, S. Abbasi, Novel photocatalytic coatings based on tin oxide semiconductor, Surface Engineering, 35 (2019) 216-226.

[12] S. Abbasi, M. Hasanpour, M.-S. Ekrami-Kakhki, Removal efficiency optimization of organic pollutant (methylene blue) with modified multi-walled carbon nanotubes using design of experiments (DOE), Journal of materials science: Materials in electronics, 28 (2017) 9900-9910.

[13] D. Meroni, R. Djellabi, M. Ashokkumar, C.L. Bianchi, D.C. Boffito, Sonoprocessing: From concepts to large-scale reactors, Chemical reviews, 122 (2021) 3219-3258.

[14] A.A. Najafpoor, M. Davoudi, E. Rahmanpour Salmani, Decolorization of synthetic textile wastewater using electrochemical cell divided by cellulosic separator, Journal of Environmental Health Science and Engineering, 15 (2017) 1-11.

[15] F. Marahel, Adsorption of hazardous methylene green dye from aqueous solution onto tin sulfide nanoparticles loaded activated carbon: isotherm and kinetics study, Iranian Journal of Chemistry and Chemical Engineering, 38 (2019) 129-142.

[16] J. Al-Abdullah, A.G. Al Lafi, T. Alnama, W. Al Masri, Y. Amin, M.N. Alkfri, Adsorption mechanism of lead on wood/nano-manganese oxide composite, Iranian Journal of Chemistry and Chemical Engineering, 37 (2018) 131-144.

[17] K.G. Akpomie, L.O. Eluke, V.I.E. Ajiwe, C.O. Alisa, Attenuation kinetics and desorption performance of artocarpus altilis seed husk for Co (II), Pb (II) And Zn (II) Ions, Iranian Journal of Chemistry and Chemical Engineering, 37 (2018) 171-186.

[18] Y. Cao, X. Li, Adsorption of graphene for the removal of inorganic pollutants in water purification: a review, Adsorption, 20 (2014) 713-727.

[19] M. Mergbi, M.G. Galloni, D. Aboagye, E. Elimian, P. Su, B.M. Ikram, W. Nabgan, J. Bedia, H.B. Amor, S. Contreras, Valorization of lignocellulosic biomass into sustainable materials for adsorption and photocatalytic applications in water and air remediation, Environmental Science and Pollution Research, (2023) 1-31.

[20] B. Hameed, J. Salman, A. Ahmad, Adsorption isotherm and kinetic modeling of 2, 4-D pesticide on activated carbon derived from date stones, Journal of hazardous materials, 163 (2009) 121-126.

[21] R. Djellabi, B. Yang, Y. Wang, X. Cui, X. Zhao, Carbonaceous biomass-titania composites with TiOC bonding bridge for efficient photocatalytic reduction of Cr (VI) under narrow visible light, Chemical Engineering Journal, 366 (2019) 172-180.

[22] N. Abderrahim, M. Mergbi, H.B. Amor, R. Djellabi, Optimization of microwave assisted synthesis of activated carbon from biomass waste for sustainable industrial crude wet-phosphoric acid purification, Journal of Cleaner Production, 394 (2023) 136326.

[23] E.H. Elkhattabi, M. Lakraimi, M. Badreddine, A. Legrouri, O. Cherkaoui, M. Berraho, Removal of Remazol Blue 19 from wastewater by zinc–aluminium–chloride-layered double hydroxides, Applied Water Science, 3 (2013) 431-438.

[24] Y. Azimzadeh, N. Najafi, A. Reyhanitabar, S. Oustan, A.R. Khataee, Modeling of phosphate removal by Mg-Al layered double hydroxide functionalized biochar and hydrochar from aqueous solutions, Iranian Journal of Chemistry and Chemical Engineering, 40 (2021) 565-579.

[25] F. Cavani, F. Trifiro, A. Vaccari, Hydrotalcite-type anionic clays: Preparation, properties and applications, Catalysis today, 11 (1991) 173-301.

[26] M. Wei, S. Shi, J. Wang, Y. Li, X. Duan, Studies on the intercalation of naproxen into layered double hydroxide and its thermal decomposition by in situ FT-IR and in situ HT-XRD, Journal of Solid State Chemistry, 177 (2004) 2534-2541.

[27] X. Feng, R. Long, L. Wang, C. Liu, Z. Bai, X. Liu, A review on heavy metal ions adsorption from water by layered double hydroxide and its composites, Separation and Purification Technology, 284 (2022) 120099.

[28] M. Daud, A. Hai, F. Banat, M.B. Wazir, M. Habib, G. Bharath, M.A. Al-Harthi, A review on the recent advances, challenges and future aspect of layered double hydroxides (LDH)–Containing hybrids as promising adsorbents for dyes removal, Journal of Molecular Liquids, 288 (2019) 110989.

[29] R.M.M. dos Santos, R.G.L. Gonçalves, V.R.L. Constantino, L.M. da Costa, L.H.M. da Silva, J. Tronto, F.G. Pinto, Removal of Acid Green 68: 1 from aqueous solutions by calcined and uncalcined layered double hydroxides, Applied clay science, 80 (2013) 189-195.

[30] R. Djellabi, R. Giannantonio, E. Falletta, C.L. Bianchi, SWOT analysis of photocatalytic materials towards large scale environmental remediation, Current Opinion in Chemical Engineering, 33 (2021) 100696.

[31] M.B. Gholivand, Y. Yamini, M. Dayeni, S. Seidi, E. Tahmasebi, Adsorptive removal of alizarin red-S and alizarin yellow GG from aqueous solutions using polypyrrole-coated magnetic nanoparticles, Journal of Environmental Chemical Engineering, 3 (2015) 529-540.

[32] Z. Abou-Gamra, Kinetics of decolorization of Alizarin Red S in aqueous media by Fenton-like mechanism, Eur. Chem. Bull, 3 (2014) 108-112.

[33] C. Zhu, C. Jiang, S. Chen, R. Mei, X. Wang, J. Cao, L. Ma, B. Zhou, Q. Wei, G. Ouyang, Ultrasound enhanced electrochemical oxidation of Alizarin Red S on boron doped diamond (BDD) anode: Effect of degradation process parameters, Chemosphere, 209 (2018) 685-695.

[34] B. Kamarehie, A. Jafari, M. Ghaderpoori, M. Amin Karami, K. Mousavi, A. Ghaderpoury, Catalytic ozonation process using PAC/γ-Fe2O3 to Alizarin Red S degradation from aqueous solutions: a batch study, Chemical Engineering Communications, 206 (2019) 898-908.

[35] J. Sun, H. Lu, L. Du, H. Lin, H. Li, Anodic oxidation of anthraquinone dye Alizarin Red S at Ti/BDD electrodes, Applied Surface Science, 257 (2011) 6667-6671.

[36] S.K. Kansal, R. Lamba, S. Mehta, A. Umar, Photocatalytic degradation of Alizarin Red S using simply synthesized ZnO nanoparticles, Materials letters, 106 (2013) 385-389.

[37] F. Fu, Z. Gao, L. Gao, D. Li, Effective adsorption of anionic dye, alizarin red S, from aqueous solutions on activated clay modified by iron oxide, Industrial & Engineering Chemistry Research, 50 (2011) 9712-9717.

[38] W.T. Reichle, Synthesis of anionic clay minerals (mixed metal hydroxides, hydrotalcite), Solid State Ionics, 22 (1986) 135-141.

[39] S. Abbasi, D. Dastan, Ş. Ţălu, M. Tahir, M. Elias, L. Tao, Z. Li, Evaluation of the dependence of methyl orange organic pollutant removal rate on the amount of titanium dioxide nanoparticles in MWCNTs-TiO2 photocatalyst using statistical methods and Duncan's multiple range test, International journal of environmental analytical chemistry, (2022) 1-15.

[40] G. Yang, H. Chen, H. Qin, Y. Feng, Amination of activated carbon for enhancing phenol adsorption: Effect of nitrogen-containing functional groups, Applied Surface Science, 293 (2014) 299-305.

[41] R. Elmoubarki, F.Z. Mahjoubi, A. Elhalil, H. Tounsadi, M. Abdennouri, M.h. Sadiq, S. Qourzal, A. Zouhri, N. Barka, Ni/Fe and Mg/Fe layered double hydroxides and their calcined derivatives: preparation, characterization and application on textile dyes removal, Journal of materials research and technology, 6 (2017) 271-283.

[42] M.R. Haider, W.-L. Jiang, J.-L. Han, A. Mahmood, R. Djellabi, H. Liu, M.B. Asif, A.-J. Wang, Boosting Hydroxyl Radical Yield via Synergistic Activation of Electrogenerated HOCl/H2O2 in Electro-Fenton-like Degradation of Contaminants under Chloride Conditions, Environmental Science & Technology, (2023).

[43] F. Djani, M. Omari, A. Martínez-Arias, Synthesis, characterization and catalytic properties of La (Ni, Fe) O 3–NiO nanocomposites, Journal of Sol-Gel Science and Technology, 78 (2016) 1-10.

[44] C.F. Li, L.J. Xie, J.W. Zhao, L.F. Gu, H.B. Tang, L. Zheng, G.R. Li, Interfacial Fe− O− Ni− O− Fe Bonding Regulates the Active Ni Sites of Ni-MOFs via Iron Doping and Decorating with FeOOH for Super-Efficient Oxygen Evolution, Angewandte Chemie International Edition, 61 (2022) e202116934.

[45] S. Abbasi, M. Hasanpour, The effect of pH on the photocatalytic degradation of methyl orange using decorated ZnO nanoparticles with SnO 2 nanoparticles, Journal of materials science: Materials in electronics, 28 (2017) 1307-1314.

[46] Y. Yang, X. Lin, B. Wei, Y. Zhao, J. Wang, Evaluation of adsorption potential of bamboo biochar for metal-complex dye: equilibrium, kinetics and artificial neural network modeling, International Journal of Environmental Science and Technology, 11 (2014) 1093-1100.

[47] Y. Cai, B. Tang, L. Bin, S. Huang, P. Li, F. Fu, Constructing a multi-layer adsorbent for controllably selective adsorption of various ionic dyes from aqueous solution by simply adjusting pH, Chemical Engineering Journal, 382 (2020) 122829.

[48] S. Halacheva, J. Penfold, R. Thomas, J. Webster, Solution pH and Oligoamine Molecular Weight Dependence of the Transition from Monolayer to Multilayer Adsorption at the Air–Water Interface from Sodium Dodecyl Sulfate/Oligoamine Mixtures, Langmuir, 29 (2013) 5832-5840.

[49] R. Zerdouma, Z. Hattabb, Y. Berredjema, R. Mazouzb, R. Djellabib, N. Filalib, A. Gheida, K. Guerfib, Removal of methylene blue from water using eggshell membrane fixed bed, Desalination and Water Treatment, 81 (2017) 252-264.

[50] A. Lahmar, Z. Hattab, R. Zerdoum, N. Boutemine, R. Djellabi, N. Filali, K. Guerfi, Dynamic sorption of hexavalent chromium using sustainable low-cost eggshell membrane, Desalin. Water Treat, 181 (2020) 289-299.

[51] P. Su, X. Gao, J. Zhang, R. Djellabi, B. Yang, Q. Wu, Z. Wen, Enhancing the adsorption function of biochar by mechanochemical graphitization for organic pollutant removal, Frontiers of Environmental Science & Engineering, 15 (2021) 1-12.

[52] P. Senthil Kumar, P.S.A. Fernando, R.T. Ahmed, R. Srinath, M. Priyadharshini, A. Vignesh, A. Thanjiappan, Effect of temperature on the adsorption of methylene blue dye onto sulfuric acid–treated orange peel, Chemical Engineering Communications, 201 (2014) 1526-1547.

[53] M.T. Yagub, T.K. Sen, S. Afroze, H.M. Ang, Dye and its removal from aqueous solution by adsorption: a review, Advances in colloid and interface science, 209 (2014) 172-184.

[54] I. Langmuir, The adsorption of gases on plane surfaces of glass, mica and platinum, Journal of the American Chemical society, 40 (1918) 1361-1403.

[55] N. Boukhalfa, M. Boutahala, N. Djebri, A. Idris, Kinetics, thermodynamics, equilibrium isotherms, and reusability studies of cationic dye adsorption by magnetic alginate/oxidized multiwalled carbon nanotubes composites, International journal of biological macromolecules, 123 (2019) 539-548.

[56] A. Khandelwal, N. Narayanan, E. Varghese, S. Gupta, Linear and nonlinear isotherm models and error analysis for the sorption of kresoxim-methyl in agricultural soils of India, Bulletin of environmental contamination and toxicology, 104 (2020) 503-510.

[57] J. Zhang, Q. Xia, X. Hong, J. Chen, D. Liu, Synthesis of layered double hydroxides with nitrate and its adsorption properties of phosphate, Water Science and Technology, 83 (2021) 100-110.

[58] P. Staroń, J. Chwastowski, M. Banach, Sorption behavior of methylene blue from aqueous solution by raphia fibers, International Journal of Environmental Science and Technology, 16 (2019) 8449-8460.

[59] A.S. Özcan, B. Erdem, A. Özcan, Adsorption of Acid Blue 193 from aqueous solutions onto BTMA-bentonite, Colloids and Surfaces A: Physicochemical and Engineering Aspects, 266 (2005) 73-81.

[60] M. Shamim, K. Dana, Efficient removal of Evans blue dye by Zn–Al–NO 3 layered double hydroxide, International Journal of Environmental Science and Technology, 15 (2018) 1275-1284.

[61] M. Fayazi, M. Ghanei-Motlagh, M.A. Taher, The adsorption of basic dye (Alizarin red S) from aqueous solution onto activated carbon/γ-Fe2O3 nano-composite: kinetic and equilibrium studies, Materials Science in Semiconductor Processing, 40 (2015) 35-43.

[62] R.K. Gautam, A. Mudhoo, M.C. Chattopadhyaya, Kinetic, equilibrium, thermodynamic studies and spectroscopic analysis of Alizarin Red S removal by mustard husk, Journal of Environmental Chemical Engineering, 1 (2013) 1283-1291.

[63] A.B. Albadarin, C. Mangwandi, Mechanisms of Alizarin Red S and Methylene blue biosorption onto olive stone by-product: Isotherm study in single and binary systems, Journal of environmental management, 164 (2015) 86-93.

[64] L. Fan, Y. Zhang, X. Li, C. Luo, F. Lu, H. Qiu, Removal of alizarin red from water environment using magnetic chitosan with Alizarin Red as imprinted molecules, Colloids and Surfaces B: Biointerfaces, 91 (2012) 250-257.

[65] H. Biglari, S. RodríguezíCouto, Y.O. Khaniabadi, H. Nourmoradi, M. Khoshgoftar, A. Amrane, M. Vosoughi, S. Esmaeili, R. Heydari, M.J. Mohammadi, Cationic surfactant-modified clay as an adsorbent for the removal of synthetic dyes from aqueous solutions, International journal of chemical reactor engineering, 16 (2018) 20170064.

[66] Y. Qiao, Q. Li, H. Chi, M. Li, Y. Lv, S. Feng, R. Zhu, K. Li, Methyl blue adsorption properties and bacteriostatic activities of Mg-Al layer oxides via a facile preparation method, Applied Clay Science, 163 (2018) 119-128.

[67] M. Abbasi, M.M. Sabzehmeidani, M. Ghaedi, R. Jannesar, A. Shokrollahi, Adsorption performance of calcined copper-aluminum layered double hydroxides/CNT/PVDF composite films toward removal of carminic acid, Journal of Molecular Liquids, 329 (2021) 115558.